Characterization of a Penning discharge for investigation of auroral radio wave generation mechanisms

2011 Plasma Phys. Control. Fusion 53 124020

(http://iopscience.iop.org/0741-3335/53/12/124020)

Plasma Phys. Control. Fusion **53** (2011) 124020 (9pp) doi:10.1088/0741-3335/53/12/124020

Characterization of a Penning discharge for investigation of auroral radio wave generation mechanisms

S L McConville[1], M E Koepke[2], K M Gillespie[1], K Matheson[1], C G Whyte[1], C W Robertson[1] and D C Speirs[1]

[1] SUPA Department of Physics, University of Strathclyde, G4 0NG, Scotland, UK
[2] Department of Physics, West Virginia University, Morgantown, WV 26506-6315, USA

E-mail: sandra.l.mcconville@strath.ac.uk

Received 23 June 2011, in final form 19 August 2011
Published 14 November 2011
Online at stacks.iop.org/PPCF/53/124020

Abstract

Auroral Kilometric Radiation (AKR), observed by satellites in the Earth's magnetosphere, is naturally generated in regions of partial plasma depletion (auroral density cavity) in the polar magnetosphere at approximately 3200 km altitude. As an electron descends through these regions of partial plasma depletion along magnetic field lines towards the Earth's ionosphere, the field lines increases and, through conservation of the magnetic moment, the electron gives up axial velocity in favour of perpendicular velocity. This results in a horseshoe-shaped distribution function in parallel/perpendicular-velocity space which is unstable to X-mode radiation, near the cyclotron frequency. Power levels as high as GW levels have been recorded with frequencies around 300 kHz. The background plasma frequency within the auroral density cavity is approximately 9 kHz corresponding to a plasma density 1 cm^{-3}. A laboratory experiment scaled from auroral frequency to microwave frequency has previously been reported. Here, the addition of a Penning trap to simulate the background plasma of the density cavity is reported, with measurements $n_e \sim 2 \times 10^{14}$–$2.17 \times 10^{15}\,m^{-3}$, $f_{pe} \sim 128$–418 MHz and $f_{ce} \sim 5.21$ GHz giving a ratio of ω_{ce}/ω_{pe} comparable to the magnetospheric AKR source region.

(Some figures in this article are in colour only in the electronic version)

1. Introduction

Magnetized planets including the Earth, and stellar objects such as UV Ceti, have been shown to produce non-thermal planetary radio emission due to cyclotron maser radiation (Bingham *et al* 2001). This emission of radiation occurs naturally at the Earth's polar regions and is known as

Auroral Kilometric Radiation (AKR). AKR has been observed, by satellites (Benediktov *et al* 1965, Gallagher and Gurnett 1979) and by ground-level instruments (LaBelle and Anderson 2011). Short-duration radio bursts at frequencies 50–800 kHz (Mutel *et al* 2004) are typical. The radiation, characterized by a peak near 300 kHz and a spectrum that extends down to the local cyclotron frequency, is observed to be in the X-mode at powers on the order of 10^9 W, corresponding to an estimated radiation efficiency of around 1% of the precipitated electron kinetic energy (Gurnett 1974, Pritchett and Strangeway 1985). The efficiency of this naturally occurring process is especially high and has led to many theoretical investigations (Bingham *et al* 1999, 2004, Vorgul *et al* 2005, Burinskaya and Rauch 2007).

The emissions originate from a region of partial plasma depletion in the Earth's polar magnetosphere, known as the auroral density cavity, having an altitude of approximately 3200 km in which $\omega_{ce}/\omega_{pe} \sim 10$–30 (Calvert 1981). Evidence has been shown for two distinct source regions of radiation generation. One of these has been observed at the lower 3200 km altitude and a second, according to recent observations, at altitudes up to 12 000 km (Morioka *et al* 2008). Particles descend through this region along a magnetic flux tube that decreases in cross-sectional area, whereby they sacrifice axial velocity for perpendicular velocity according to the adiabatic invariant μ and the conservation of total energy. This creates a distribution in velocity space which resembles a horseshoe (Delory *et al* 1998, Ergun *et al* 1998, Bingham and Cairns 2000, 2002). The principal features of this process have been replicated in the laboratory (Speirs *et al* 2005, McConville *et al* 2008, Ronald *et al* 2008, 2011) and in numerical simulations (Cairns *et al* 2005, 2011, Gillespie *et al* 2008, Speirs *et al* 2008, 2010, Vorgul *et al* 2011). An important step in simulating AKR-scaled conditions in the laboratory is providing the scaled background plasma observed in the magnetosphere. This is relevant as the presence of the background plasma is predicted to affect the emission process due to the proximity of the emission signal to the upper hybrid resonance (Allen and Phelps 1977). In this paper, a background plasma is created through a low density 'collisionless' discharge as a new essential element in the laboratory experimental configuration.

2. Apparatus

2.1. Magnet coils and electron injector

Figure 1(*a*) shows the experimentally measured magnetic field profile, the magnitude of which can be precisely tuned by independent control of five solenoids. The beam is injected at the left side of figure 1(*a*) with a small initial spread in velocity, by virtue of the gun design figure 1(*b*), into the 16 cm diameter anode can. The anode mesh is shown in figure 1(*c*). The line at (i) in figure 1(*a*) shows the position of the cathode face whilst the line at (ii) shows the mid-point of the interaction waveguide (McConville *et al* 2008).

2.2. Quasi-Penning trap design

The plasma confinement region used a design derived from a Penning trap (figure 2(*a*)). The Penning cavity was based on the conventional design of two solid cathodes and a cylindrical anode creating a trap in which electrons are confined. This experiment is designed so that an electron beam passes along the magnetic axis (z-axis) of the apparatus and through a 40 mm hole cut in one cathode plate (figure 2(*b*)). The second cathode plate was replaced with a mesh to allow egress of radiation. The mesh (figure 2(*c*)) has radially oriented wires which are transparent to the purely azimuthally polarized electric fields of the intended TE_{01} mode. To test the properties of the mesh and ensure that it would allow for TE_{01} mode egress, a Marie

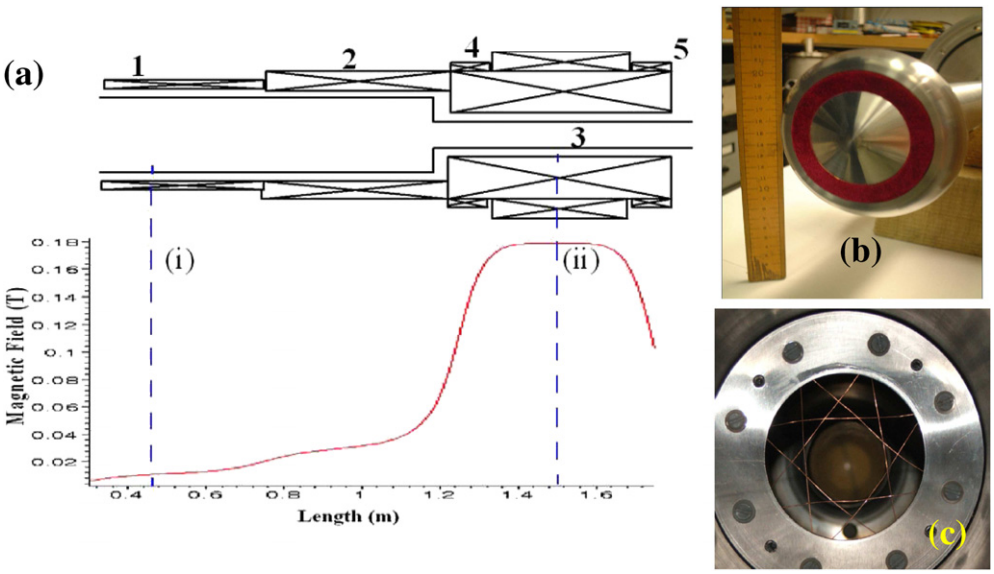

Figure 1. (*a*) Magnet coils and measured magnetic field profile, (*b*) cathode dome face with velvet ring, (c) anode mesh showing copper wires.

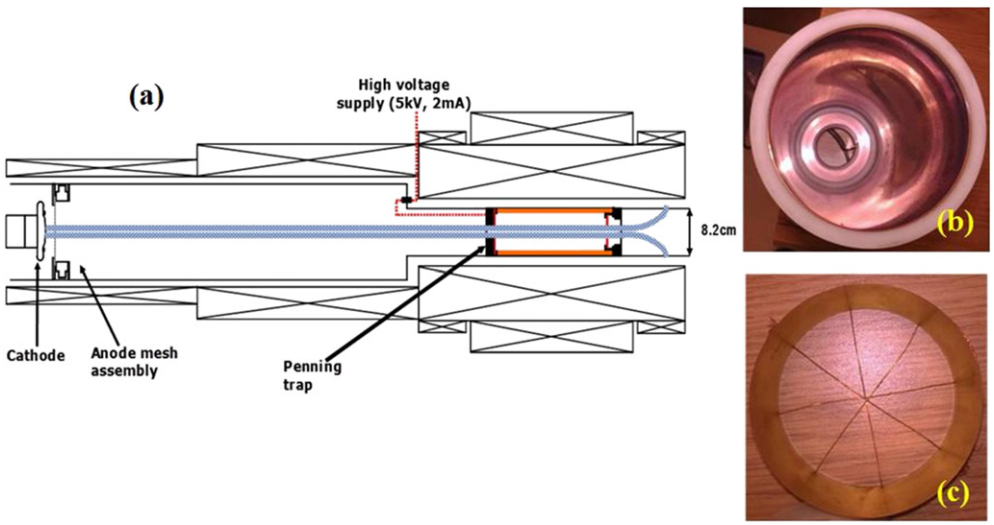

Figure 2. (*a*) Schematic showing the position of the Penning trap and high voltage connection, (*b*) view through the Penning trap to the gun-end cathode with 40 mm diameter hole, (*c*) cathode mesh showing the spoke design for TE_{01} mode egress.

Converter was used to launch a TE_{01} test signal into the mesh that attached to the output end of the converter. Transmission and reflection measurements were made with vector and scalar network analysers and showed that the mesh did not affect the radiation egress.

The cathode and anode walls of the trap were constructed using copper; the cathodes were grounded to the external waveguide structure whilst the exterior of the anode was encased in an insulating nylon jacket to prevent the copper from touching the walls of the interaction waveguide (figure 2(*b*)). Also shown in figure 2(*a*) is a specially designed compact vacuum

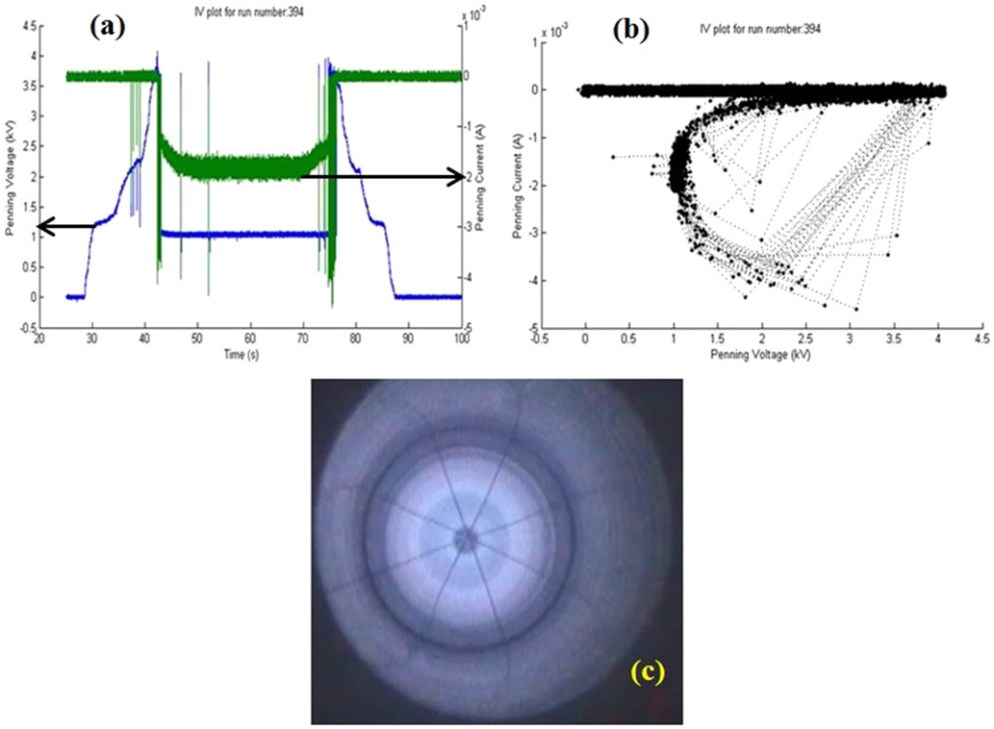

Figure 3. Voltage and current traces for the Penning discharge ignition.

feed-through capable of introducing a high voltage (up to +5 kV) to the anode. The plateau magnetic field was set at 0.21 T to achieve a near cut-off resonance between the energetic electrons from the electron gun and the TE_{01} mode of the 7.02 cm diameter interaction region.

3. Preliminary Penning trap/discharge characterization

Prior to attempting to insert any probes into the plasma, experiments were conducted to test the stability and ignition conditions for the discharge as a function of the background gas, gas pressure and magnetic field. Measurements initially began with three different test gases, nitrogen, argon and helium. Nitrogen gave unstable results showing obvious bimodal behaviour, regardless of the magnetic field and pressure settings, with the current and voltage of the discharge alternating rapidly between high V and low I to low V and high I. To avoid this instability, all further experiments were carried out with argon and helium.

Experiments showed that the most stable discharge at the desired magnetic field was achieved using argon at a pressure of 1×10^{-4} mbar yielding highly reproducible characteristic I–V plots (figure 3(a)). The blue trace shows the Penning voltage, whilst the green trace represents the Penning current. Here, the voltage increases across the Penning trap and at a maximum point, typically 4.2 kV, the ignition of the discharge is detected by the sudden increase in current and drop in voltage. The power supply for the Penning trap was rated to 5 kV and 3 mA. However, during the discharge ignition phase, a steady sustaining voltage in the range 0.5–1 kV was maintained. Once the discharge ignited, the voltage on the trap was only weakly affected by the supply output power, whereas the supply could readily regulate

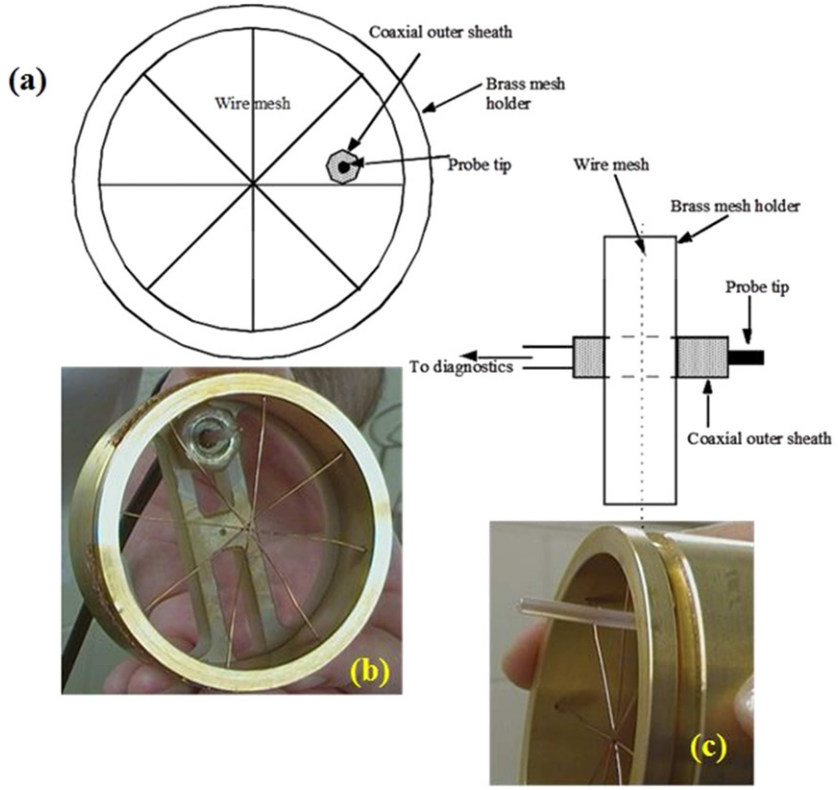

Figure 4. Schematic and visual of the cathode mesh with a nylon probe holder, showing the barrel and planar-face probe tip.

the discharge current. Figure 3(*b*) shows the processed data from figure 3(*a*) which illustrates a regime of negative differential resistance. A video camera was set up at the output window of the experiment showing the azimuthal symmetry and radial structure of the ignited discharge (figure 3(*c*)) the view being taken through the cathode mesh and along the z-axis towards the electron gun.

4. Probe design and implementation

A 10 mm section of the outer sheath of a coaxial cable was pared back to leave a section of copper wire (figure 4(*a*)). To accurately and reproducibly hold the probe in place within the interaction waveguide, a nylon slider was machined to fit into the Penning trap's cathode mesh (figure 4(*b*)). The slider allowed the radial position of the probe to be adjusted as necessary. The plasma formed in a ring around the centre of the Penning trap (figure 3(*c*)) and so the probe was placed to be in the middle of the illuminated region, as can be seen from figure 4.

A 10 mm long barrel probe was initially inserted a distance of 10 cm into the trap; this technique was quickly abandoned as the probes presence, prior to discharge ignition, badly affected the electrostatics of the system to the extent that the discharge ignition failed. The probe was repositioned just inside the mesh, greatly reducing the electrostatic disruption and thus allowing the discharge to be ignited. It is noted that, to ignite the discharge with the probe present, it was essential to use helium gas instead of argon with an operating pressure

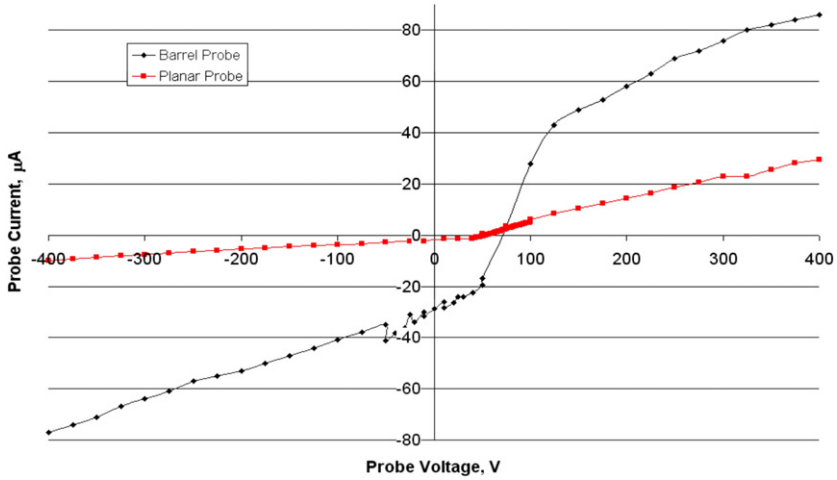

Figure 5. Difference in current dependent on the geometry of the probe tip.

exceeding 1×10^{-4} mbar. In these cases the discharge, with $B = 0.21$ T, had quantitatively similar I–V characteristics irrespective of the presence of the probe.

The helical orbits of magnetized-plasma particles complicate the interpretation of their collection onto the probe tip. This can be seen in figure 5 illustrating the collected probe current for two different probe geometries; a barrel tip of length 10 mm (figure 4(*b*)) and a planar-face tip, flush with the nylon outer sheath (figure 4(*c*)). The collection areas for the barrel and planar probe are 2.01×10^{-5} m^2 and 6.2×10^{-7} m^2, respectively, a ratio of 30. The maximum collected current for the barrel and planar probe was 85 μA and 30 μA, respectively, a ratio less than 3. This shows that the cylindrical surface of the barrel probe dominated the current collection but not by the factor of 30 implied by the increased collection area. The planar probe was better suited for primarily longitudinal current collection and was therefore used for plasma measurements.

5. Discharge characterization with plasma probe diagnostic

To mitigate some of the uncertainties inherent in applying simple probe theory to measured I–V characteristic curves of a plasma in the presence of the magnetic field (Brown *et al* 1971, Zimmermann *et al* 2009) two procedures were used to analyse the experiment. One was to analyse the I–V characteristics according to simple Langmuir probe theory (section 5.1). The second was to measure the spectrum of oscillations at the tip of the floating probe (section 5.2) thereby directly measuring the plasma oscillations.

5.1. 'Langmuir probe' and Bohm sheath analysis

Measurements of current density and probe bias voltage, i.e. the difference between the applied probe voltage and the plasma's space potential as measured by a floating probe, were obtained allowing a plot of Ln J versus V to be formed as shown in figure 6.

Using equation (1), one can infer the temperature of the plasma electrons, assuming purely axial drift of the particles near the probe, assuming a one-temperature electron energy

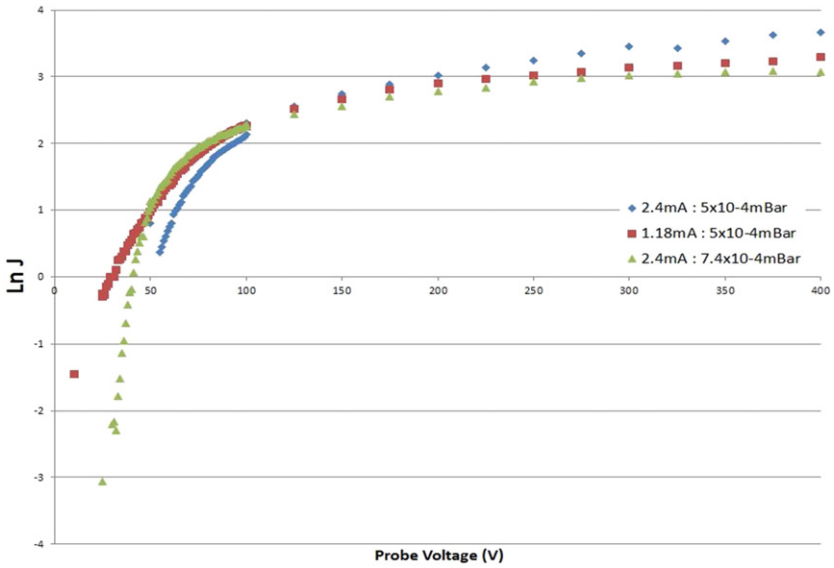

Figure 6. This logarithmic plot of the current density allowed T_e to be inferred and consequently ω_{pe} of the plasma was experimentally estimated.

distribution, and ignoring the magnetic field effects,

$$\mathrm{Ln}\, J = \mathrm{Ln} J_0 + \frac{eV_{pr}}{kT_e} \tag{1}$$

where V_{pr} is the voltage applied to the probe and (e/kT_e) is the value of the slope of the steep section of figure 6. From this characterization, the temperature, number density and plasma frequency and their uncertainties could be experimentally estimated. Since simple probe theory does not include a magnetic field and modelling magnetic field effects significantly complicates the analysis, a second estimate of number density was obtained using Bohm sheath theory. This method determined the ion density using both the probe's estimate of electron temperature and the area of the discharge cathode as the ion collection surface for the total discharge current.

Using probe theory, the following estimates were obtained; $7.5 \times 10^{14} < n_e < 2.17 \times 10^{15}\,\mathrm{m}^{-3}$, $5.51 \times 10^4 < T_e < 2.48 \times 10^5\,\mathrm{K}$ and $245 < f_{pe} < 418\,\mathrm{MHz}$. Using Bohm theory f_{pe} was estimated to be in the range 128–266 MHz.

5.2. Using probe as a direct resonance pickup antenna

Connecting the plasma probe to a spectrum analyser allows it to be utilized as a direct antenna pickup. Figure 7 shows the spectrum of plasma oscillations measured by the analyser within the vicinity of the probe, from zero frequency to some well-defined maximum frequency that varied approximately as $\sqrt{I_A}$. Implied here is that as the distance away from the probe increases, the number density, and consequently the plasma frequency, increases until, upon reaching the probe sheath boundary, the maximum plasma frequency of the bulk plasma was observed. Any higher frequencies at this point are uncoupled to the plasma and cannot be sustained in the properties of the interaction waveguide.

According to the graph, as the current applied to the Penning trap increases from 0.8 to 2.5 mA, the measured cut-off frequency increases from ~220–320 MHz, a range that is comparable to the estimated range of plasma frequencies using probe and Bohm theory.

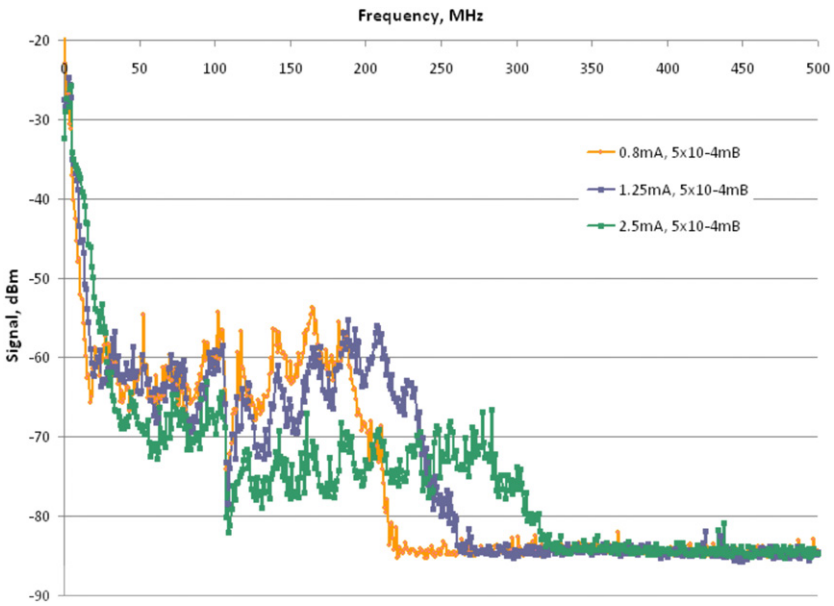

Figure 7. Direct plasma frequency measurements using the probe as an antenna pickup.

Although the density of the plasma has thus far only been measured at one point, it is assumed that the plasma extends the length of the Penning trap in a cylindrical fashion of uniform density. This looks to be the case from the video images illustrated by the still in figure 3(*c*). This theory is due to be tested at a later stage with more advanced probing diagnostics.

6. Discussion/conclusion

In this paper, a background plasma is created through a low density 'collisionless' discharge as a new essential element in an AKR-related laboratory experiment, improving the comparison of laboratory experimental results to magnetospheric observations of AKR. The range of plasma density in the *in situ* discharge was found to suitably replicate the scaled conditions of the AKR source region. Three methods of plasma characterization were used and the results for the plasma frequencies and number densities of electrons; $f_{\mathrm{pe}} \sim 128$–418 MHz and $n_{\mathrm{e}} \sim 10^{14}$–$10^{15}$ m^{-3}, agreed within the experimental uncertainty. The precision achieved here is sufficient for a quantitative analysis of AKR-scaled conditions in the laboratory incorporating the scaled background plasma observed in the magnetosphere and the assessment of the effect of the background plasma on the emission process due to the proximity of the emission signal to the upper hybrid resonance.

Acknowledgments

The authors would like to thank the EPSRC and STFC Centre for Fundamental Physics who supported this work. Mr David Barclay and Mr Iain Dinwoodie are thanked for their help in creating the apparatus.

References

Allen J E and Phelps A D R 1977 *Rep. Prog. Phys.* **40** 1305–68
Benediktov E A, Getmantsev G G, Sazonoy Y A and Tarasov A F 1965 *Kosm. Issled* **3** 614–17
Bingham R and Cairns R A 2000 *Phys. Plasmas* **7** 3089–92
Bingham R and Cairns R A 2002 *Phys. Scr.* **T98** 160–2
Bingham R, Cairns R A and Kellett B J 2001 *Astron. Astrophys.* **370** 1000–3
Bingham R, Kellett B J, Cairns R A, Dendy R O and Shukla P K 1999 *Geophys. Res. Lett.* **26** 2713–6
Bingham R, Kellett B J, Cairns R A, Vorgul I, Phelps A D R, Ronald K and Speirs D C 2004 *Contrib. Plasma Phys.* **44** 382–7
Brown I G, Compher A B and Kunkel W B 1971 *Phys. Fluids* **14** 1377–83
Burinskaya T M and Rauch J L 2007 *Plasma Phys. Rep.* **33** 28–37
Cairns R A, Speirs D C, Ronald K, Vorgul I, Kellett B J, Phelps A D R and Bingham R 2005 *Phys. Scr.* **T116** 23–6
Cairns R A *et al* 2011 *Phys. Plasmas* **18** 022902
Calvert W 1981 *Geophys. Res. Lett.* **8** 919–21
Delory G T *et al* 1998 *Geophys. Res. Lett.* **25** 2069
Ergun R E *et al* 1998 *Geophys. Res. Lett.* **25** 2061
Gallagher D L and D A Gurnett 1979 *J. Geophys. Res.* **84** 6501
Gillespie K M *et al* 2008 *Plasma Phys. Control. Fusion* **50** 1–11
Gurnett D A 1974 *J. Geophys. Res.* **79** 4227–38
LaBelle J and Anderson R R 2011 *Geophys. Res. Lett.* **38** L04104
McConville S L *et al* 2008 *Plasma Phys. Control. Fusion* **50**
Morioka A *et al* 2008*J. Geophys. Res.* **113** A09213
Mutel R L, Gurnett D A and Christopher I W 2004 *Ann. Geophys.* **22** 2625–32
Pritchett P L and Strangeway R J 1985 *J. Geophys. Res.—Space Phys.* **90** 9650–62
Ronald K *et al* 2008 *Plasma Sources Sci. Technol.* **17** 1–8
Ronald K *et al* 2011 *Plasma Phys. Control. Fusion* **53** 074015
Speirs D C *et al* 2005 *J. Plasma Phys.* **71** 665–74
Speirs D C *et al* 2008 *Plasma Phys. Control. Fusion* **50** 1–15
Speirs D C *et al* 2010 *Phys. Plasmas* **17** 056501
Vorgul I, Cairns R A and Bingham R 2005 *Phys. Plasmas* **12** 1–8
Vorgul I, Kellett B J, Cairns R A, Bingham R, Ronald K, Speirs D C, McConville S L, Gillepsie K M and Phelps A D R 2011 *Phys. Plasmas* **18** 056501
Zimmermann T M G, Coppins M and Allen J E 2009 *Phys. Plasmas* **16** 043501